

Real-Time “Eye-Writing” Recognition Using Electrooculogram

Kwang-Ryeol Lee, Won-Du Chang, Sungkean Kim, and Chang-Hwan Im, *Member, IEEE*

Abstract—Eye movements can be used as alternative inputs for human-computer interface (HCI) systems such as virtual or augmented reality systems as well as new communication ways for patients with locked-in syndrome. In this study, we developed a real-time electrooculogram (EOG)-based eye-writing recognition system, with which users can write predefined symbolic patterns with their volitional eye movements. For the “eye-writing” recognition, the proposed system first reconstructs the eye-written traces from EOG waveforms in real-time; then, the system recognizes the intended symbolic inputs with a reliable recognition rate by matching the input traces with the trained eye-written traces of diverse input patterns. Experiments with 20 participants showed an average recognition rate of 87.38% (F1 score) for 29 different symbolic patterns (26 lower case alphabet characters and three functional input patterns representing Space, Backspace, and Enter keys), demonstrating the promise of our EOG-based eye-writing recognition system in practical scenarios.

Index Terms—Assistive devices, biomedical signal processing, electrooculography (EOG), human-computer interaction (HCI), pattern analysis, rehabilitation.

I. INTRODUCTION

HUMANS use voluntary eye movements to fixate and track visual stimuli [1], [2], and healthy individuals can control their eye movements of their own volition [2]. The modern eye tracking technologies have allowed human eye movements to be used as an input modality for human-computer interaction (HCI) applications [3]. For example, Kaufman *et al.* designed a command input system in which the horizontal and vertical movements of the users' eyes were used to select a menu item from a 3×2 boxed menu on a computer screen [4]. Tomita *et al.* proposed a system where a mouse cursor on a computer monitor could be controlled by users' voluntary

eye movements, and a desired item at which the cursor was pointed could be selected by rapidly blinking their eyes [5]. Wijesoma *et al.* developed an assistive mobile robot controller using saccadic eye movements and eye blinks [6]. Deng *et al.* implemented several eye movement-based HCI applications such as a TV remote controller, a game, and an eyesight test application [7].

One of the possible applications of these eye movement-based HCI systems is a communication platform for patients with amyotrophic lateral sclerosis (ALS), generally known as Lou Gehrig's disease. ALS is a neurodegenerative disease characterized by the progressive loss of motor neurons in the brain [8]. Patients with ALS suffer from progressive paralysis of the muscles of the limbs and trunk, as well as those used for speech. Thus, patients with severe ALS cannot use their hands or voices to communicate with other people. Nevertheless, the muscles associated with eye movements are less affected by ALS than are other muscles, as the oculomotor nuclei are believed to be resistant to the neurodegenerative effects of ALS due to the increased GABAergic transmission [9]. Therefore, eye movements can be utilized as an alternative communication way for patients with ALS. Indeed, an optical eye tracker-based “eyeball mouse” is the most popular device for patients with ALS to communicate with their caregivers and computers.

To implement an eye movement-based HCI system, the video-based measurement of eye locations has been most widely used. Video-based eye tracking methods use reflected light from the eyes, which can be detected by an optical sensor or a camera [10], [11]. These methods provide very sensitive and accurate estimations of gaze directions compared with other eye tracking methods. However, this type of sensing requires ample image processing; thus, its computational cost is higher than those of other methods. In addition, some devices based on this sensing method not only occlude a part of the user's view, but also are influenced by surrounding illumination [12], [13]. Electrooculogram (EOG)-based eye tracking is an alternative to video-based eye tracking. EOG refers to the electric potentials recorded around the eyes and reflects changes in eye positions. In contrast to the video-based eye trackers, EOG-based eye trackers require relatively lower computational power, and they are not influenced by ambient lighting conditions [14]. Consequently, EOG can be used to develop relatively low-cost and low-power embedded eye-tracking systems for various purposes such as wheelchair controllers [15], [16], communication (typing) systems [17], and human activity monitoring

Manuscript received November 04, 2015; revised January 19, 2016; accepted March 10, 2016. Date of publication March 15, 2016; date of current version January 06, 2017. This work was supported by the National Research Foundation of Korea (NRF) grants funded by the Korea government under Grant NRF-2014R1A1A2A16052334, Grant NRF-2015M3C7A1031969, and Grant 2014R1A2A1A11051796. K.-R. Lee and W.-D. Chang contributed equally to this work. *Corresponding author: Chang-Hwan Im* (e-mail: ich@hanyang.ac.kr).

K.-R. Lee is with the Department of Bio and Brain Engineering, Korea Advanced Institute of Science and Technology, Daejeon 305-701, Korea.

W.-D. Chang, S. Kim, and C.-H. Im are with the Department of Biomedical Engineering, Hanyang University, Seoul, 04763 Korea (e-mail: ich@hanyang.ac.kr).

Color versions of one or more of the figures in this paper are available online at <http://ieeexplore.ieee.org>.

Digital Object Identifier 10.1109/TNSRE.2016.2542524

systems with wearable EOG goggles [18]. In this study, the EOG-based eye tracking method was exploited.

As aforementioned, HCI systems based on EOG-based eye tracking utilize various features such as the start and end times of eye movements [15]–[18], eye blinks [17], [18], and course directional change in gaze [17], [18]. Although these systems might be useful in some applications, they have limitations in providing diverse input patterns to general HCI systems. One of the alternative methods to generate more numbers of input patterns is to recognize and classify “eye-writing” patterns from EOG signals recorded while users are writing predefined symbolic trace patterns corresponding to specific commands. The feasibility of the eye-writing-based communication system was studied by Tsai *et al.* [19]. They used coarse directional changes in gaze (gaze turn counts) during eye-writing as inputs for artificial neural networks, instead of using the exact eye-written traces. Their study showed that a computer system could recognize 14 different eye-writing patterns (ten Arabic numerals and four arithmetic operators) with an average recognition accuracy of 72.1%.

In this paper, we developed a new real-time, EOG-based eye-writing recognition system. The differences between our system and the conventional EOG-based HCI systems are as follows: First, in our system, eye-written traces are reconstructed from the EOG signal in real time based on the relationship between gaze position and EOG amplitude. The reconstructed eye-written traces are then utilized as an input for HCI. Although there have been previous studies on the estimation of single, momentary movement of the eyes using EOG, methods to continuously track eye movements and estimate eye movement patterns in real time have not been reported. Another uniqueness of our system is that the users' intended inputs are recognized by applying waveform matching algorithms to the eye-written traces. Such an approach has been generally used for hand-writing recognition problems but has never been applied to eye-writing recognition applications. Our online experiments showed that the proposed system can yield reliable recognition rates of eye-writing even with diverse input patterns (29 patterns: 26 lower case alphabet characters and three functional input patterns representing Space, Backspace, and Enter keys). Our eye-writing recognition system can not only be used for a variety of HCI applications such as a control system for virtual reality glasses, but also potentially provide a novel way of communication to patients with locked-in syndrome (LIS) as the users can communicate with computer systems by simply eye-writing specific commands.

II. METHODS

The overall experimental procedure is composed of three stages: preprocessing, gaze reconstruction, and classification (Fig. 1). In the preprocessing stage, two EOG components (horizontal and vertical) were acquired from the electrodes attached around the eyes, and noise and artifacts were removed from the raw signal. The next stage is gaze reconstruction. The relationship between EOG amplitude and eyeball rotation angle was estimated at this stage. This relationship was then used to calculate rotation angles of the eyeballs based on the EOG amplitude. Finally, users were instructed to eye-write

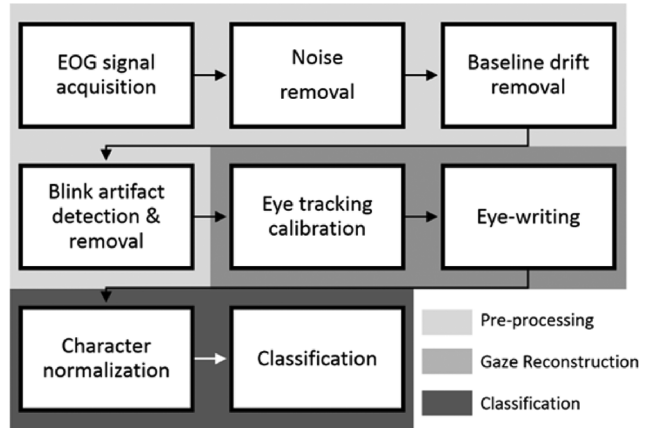


Fig. 1. Schematic diagram of the whole experimental procedure. Each block represents a single procedure, and the whole procedure can be classified into three distinct stages of preprocessing (light gray), gaze reconstruction (medium gray), and classification (dark gray).

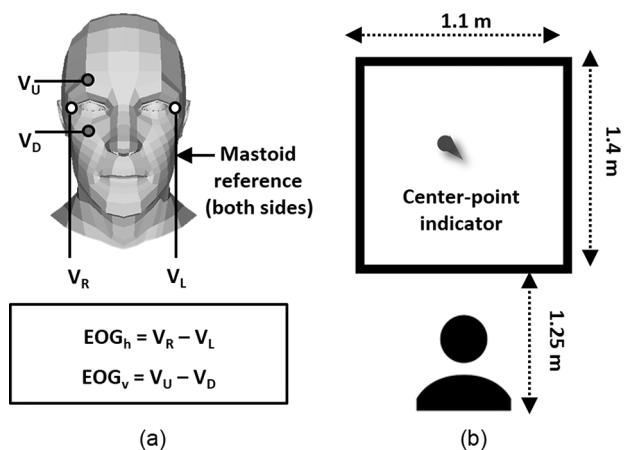


Fig. 2. Experimental settings: (a) Electrode placements and computation of two EOG components. (b) Experimental setup.

29 characters, during which classifiers based on waveform matching algorithms recognized the eye-written patterns.

A. Preprocessing

1) *EOG Signal Acquisition*: Two EOG components (horizontal and vertical) were obtained from four electrodes attached around the eyes; these were located at the outer edges of both eyes as well as above and below the right eye [Fig. 2(a)]. To reduce the computational cost of the system, four-channel EOG signals were down-sampled to a rate of 128 Hz without high-pass filtering. The horizontal EOG component was derived by subtracting the left eye signal from the right eye signal. The vertical EOG component was obtained by subtracting the signal at the lower edge of the eye from the signal at the upper edge of the eye. EOG_h and EOG_v are notations indicating the horizontal and vertical components of EOG, respectively [Fig. 2(a)].

2) *Noise Filtering*: An EOG signal contains various noise components such as thermal noise, conductance fluctuation, and power noise, as well as signal fluctuations resulting from electroencephalogram (EEG), electromyography (EMG), and electrocardiography (ECG). To minimize noise, a median filter with a fixed window size was applied to the raw EOG signal.

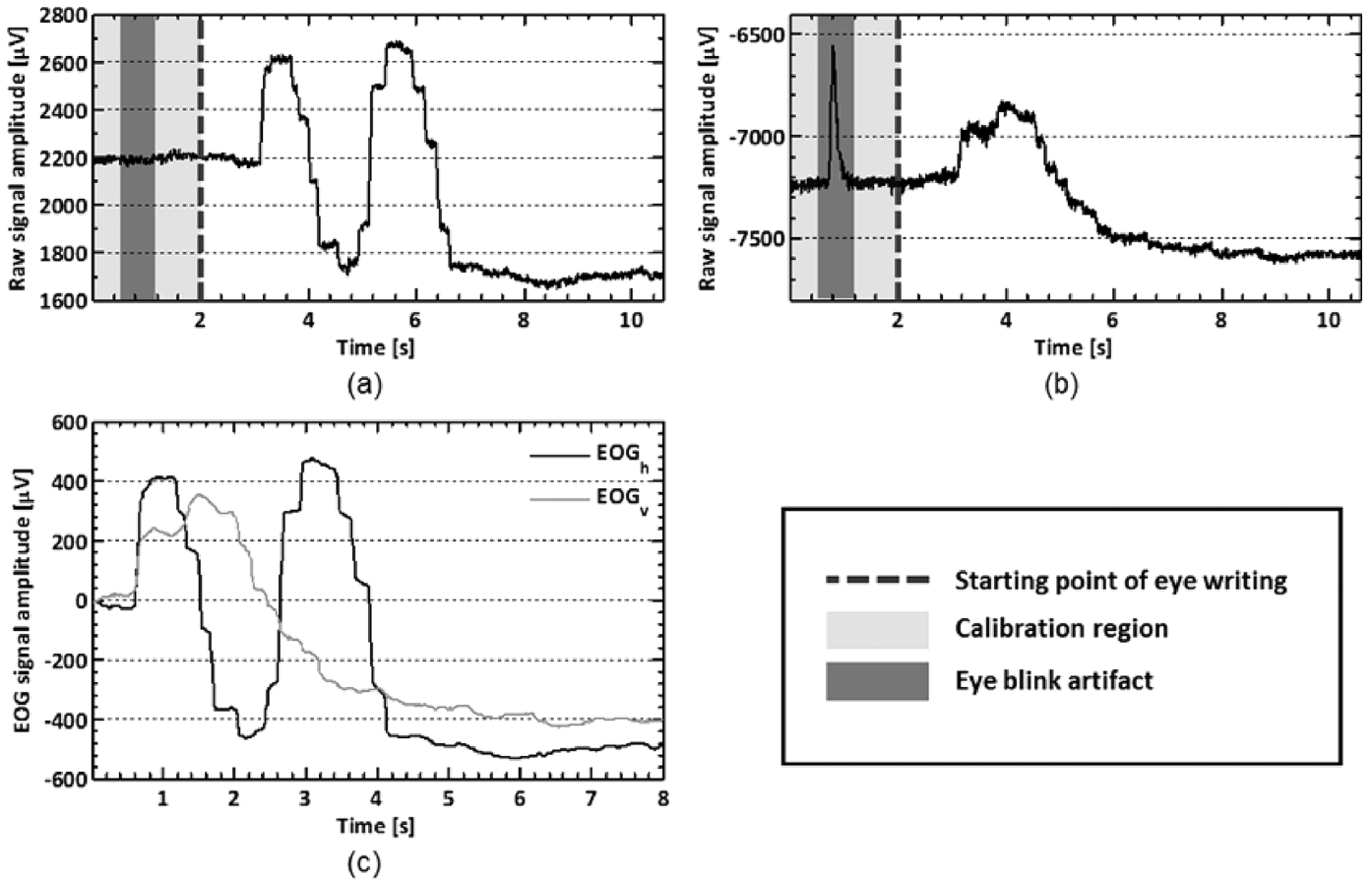


Fig. 3. Preprocessing of EOG signal. (a) Raw horizontal EOG signal. (b) Raw vertical EOG signal. (c) Preprocessed signal of an exemplar letter “s”. Users were instructed to focus on a single center point for two seconds prior to eye-writing for eight seconds for purposes of center-point calibration. The calibration region is marked in light gray, and the eye blink artifact is marked in dark gray.

The window size of the median filter was chosen to be 20 points, which was equivalent to 160 milliseconds. Since a median filter removes pulses with a width smaller than about half of its window size [18], the window size should be large enough to preserve the microstructures in the signal, which contain information about rapidly changing eye movements such as blinking. A visual inspection of the filtered signal confirmed that the selected window size was effective for removing noise while preserving the eye movement-related microstructures.

3) *Baseline Drift Removal*: The shifting resting potentials (baseline drift) of EOG make it challenging to estimate eye-rotation angles from EOG amplitudes. Therefore, the baseline drift should be removed from the original EOG signal. A typical approach is to model the baseline drift as a polynomial function [20]. In this study, we modeled the drift with a linear function (i.e., a polynomial function with degree one) as the resting potential linearly increased or decreased during a short period of time (while a user wrote one character with eye movements). Users were instructed to focus on a single center point for two seconds prior to every eye-writing process. During this calibration period, the EOG signal was recorded and then fitted to a linear function. We refer to this process as center-point calibration. The fitted function was then used for the following eight seconds for eye-writing data acquisition. The extrapolation of the fitted function was subtracted from the raw EOG signal to

remove baseline drift from the raw signal. In this way, the signal could be zero-centered, i.e., the baseline drift could be removed (see Fig. 3).

4) *Eye Blink and Muscular Artifacts Detection and Removal*: Eye blink contaminates EOG signals in such a way that a spike signal is formed in the vertical component of the EOG [21], and this could result in unwanted upward and downward strokes during eye-writing. To remove this artifact, a fast eye blink detection algorithm, which was successfully applied to a real-time application, called the *maximum summation of first derivative within a window* (MSDW) was used [22]. The method sums the first-order derivatives of the vertical EOG signal within a sliding window. The summation of first derivatives within a window (SDW) can be expressed as follows:

$$\text{SDW}(t) = \sum_{k=t-N+1}^t \{ \text{EOG}_v(k) - \text{EOG}_v(k-1) \} \quad (1)$$

where N is the width of the sliding window, and t is a specific time. The detailed procedures including individual spike thresholding, eye blink judgement, and spike range determination can be found in the recent literature [23].

In addition to eye blinks, movement of facial muscles can also be an artifact source especially when subjects are frowning

[24]. This type of artifact could be removed using two unique characteristics of the artifact: 1) a plateau-like waveform in both horizontal and vertical EOG signals, i.e., the amplitudes of horizontal and vertical EOGs increase at the same time, sustain flat while frowning, and then decrease again to the previous amplitudes as subjects stop frowning; and 2) maximum amplitudes exceed the normal range of EOG signal ($\pm 800 \mu\text{V}$). Afterwards, the data samples within the artifact contaminated regions were removed from the signal and ignored in further procedures.

B. Gaze Reconstruction

1) *Determination of Transfer Function Between EOG Amplitude and Eye-Rotation Angle*: The horizontal and vertical eye-rotation angles can be deduced from the amplitude of their respective EOG components once the relationship (transfer function) between the EOG amplitude and eye-rotation angle is determined. EOG signal amplitude and eye-rotation angle are known to have a linear relationship within the boundary of 30 degrees of eye-rotation angle [24], [25], in which the relationship can be explained as a linear function in a 3-D plane. However, the parameters of the function should be determined through a calibration process, as it varies from person to person and with different electrode attachment positions. To determine the parameters, we utilized the multiple-point calibration (MPC) method proposed by Yagi *et al.* [27] and Lee *et al.* [28]: Yagi *et al.* introduced a method to calibrate 1-D movements of the eyes (either horizontal or vertical), and Lee *et al.* introduced a method to eliminate the influence of facial angle and position. The target angle was set, and the visual stimulus (dot) was shown on the screen at the target angle position. Participants were instructed to focus on the dot without moving their heads. The preprocessed EOG output was recorded at the same time as the target angle of the stimulus. The same process was repeated N_{MPC} (the number of calibration dots) times with different calibration dot locations.

In our experiment, the target angles of each calibration point were defined as x and y (where x is the horizontal rotational angle, and y is the vertical rotational angle of the eyes), and a 3×3 uniformly distributed matrix of dots with an inter-dot-angle of 14 degrees (i.e., $N_{\text{MPC}} = 9$) was used. The recording time for each calibration point was set to three seconds.

The relationship between EOG amplitude and eye-rotation angle was determined individually using the prerecorded EOG amplitudes at certain target angles. Differences in scaling, rotation, and origin between the EOG signal and the actual gaze location can exist [28], where the possible causes of the rotational difference are unwanted crosstalk between the horizontal and vertical components of EOG and slightly tilted electrode placements due to inter-subject variability in skull structure. As linear transformations can compensate for scaling, rotation, and origin differences, the relationship can be expressed as linear equations

$$\text{EOG}_h = t_1 \cdot x + t_2 \cdot y + c_h \quad (2)$$

$$\text{EOG}_v = t_3 \cdot x + t_4 \cdot y + c_v \quad (3)$$

where $t_1, t_2, t_3, t_4, c_h,$ and c_v are all constants.

In (2) and (3), t_2 and t_3 would be zero if there is no correlation between horizontal/vertical EOG amplitudes and the

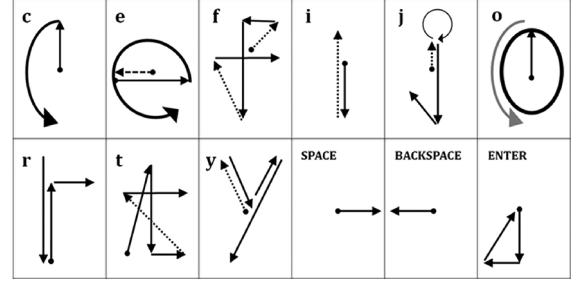


Fig. 4. Predefined eye-writing symbols used in this work. The stroke order was designed to enhance the classification accuracy. Excepting these 12 symbols, the users were instructed to write the symbols naturally with their eye movement as if they were writing original handwritten characters. The dotted lines in the figures are also parts of the actual eye movements, while the bold lines represent the original character shapes. All traces start from the point marked with a small dot.

perpendicular counterpart eye-rotation angle. These can reduce the effect of horizontal or vertical eye movement on the perpendicular counterpart EOG component. In addition, c_h and c_v would be zero if both the EOG signal amplitude and the eye-rotation angle are zero-centered. Thus, these constants are needed to compensate for the origin difference.

All constants can be determined through the linear fitting of the data points. In other words, by plotting every calibration point ($x, y, \text{EOG}_h,$ or EOG_v) on a single 3-D space and fitting the points to a linear surface, we can determine the equations of the planes for EOG_h and EOG_v , respectively. More concisely, the equation can be expressed as

$$\mathbf{EOG} = T\mathbf{x} + \mathbf{c},$$

where

$$\mathbf{EOG} = \begin{bmatrix} \text{EOG}_h \\ \text{EOG}_v \end{bmatrix}, \quad \mathbf{x} = \begin{bmatrix} x \\ y \end{bmatrix},$$

$$T = \begin{bmatrix} t_1 & t_2 \\ t_3 & t_4 \end{bmatrix}, \quad \text{and } \mathbf{c} = \begin{bmatrix} c_h \\ c_v \end{bmatrix}$$

$$\text{then, } \mathbf{EOG} = T\mathbf{x} + \mathbf{c} \quad (4)$$

where the matrix T is defined as a transfer function. In this work, $\mathbf{c} = \mathbf{0}$, because the EOG signal is zero-centered after the baseline drift removal process (i.e., the signal is calibrated to be $\mathbf{EOG} = \mathbf{0}$ when $\mathbf{x} = \mathbf{0}$). The equation then becomes

$$\mathbf{EOG} = T\mathbf{x}. \quad (5)$$

Through the MPC method described previously, the transfer function (T) can be determined. Please note that this calibration is required only one time for each experiment, as the relationship does not change over the elapsed time [27].

2) *Gaze Reconstruction and Eye-Writing Symbols*: The users' gaze positions can be reconstructed from the EOG amplitudes using the inverse of the transfer function determined from the previous step

$$\mathbf{x} = T^{-1}\mathbf{EOG}. \quad (6)$$

Users can write symbols with their eye movements while their gaze position is tracked according to (6). The resultant

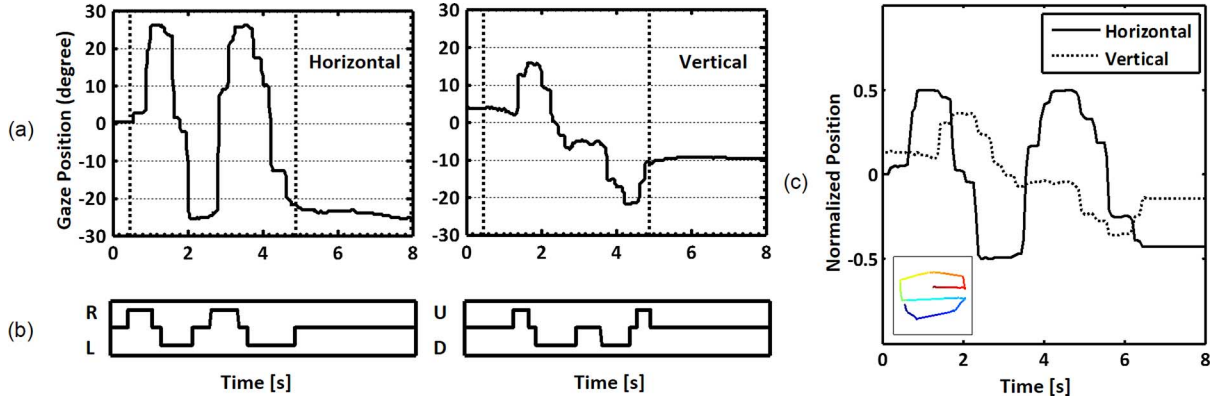


Fig. 5. Normalization of eye-written trace. (a) Changes in horizontal and vertical gaze angles when a user eye-wrote the letter “s”. The dotted black lines in the two gaze position graphs indicate truncated ranges. (b) Detected movement during the eye-writing period. (c) Truncated and normalized eye-written traces. The lower left box contains the reconstructed eye-written symbol from the normalized trace. Its colors indicate the stroke order (from red to blue).

time-series data of the gaze traces are then collected, which we will refer to as the “eye-written trace.”

The symbols used for eye-writing included 26 lower case letters and three functional symbols: Space, Backspace, and Enter keys. Users were instructed to write lower case alphabets as if they were writing original handwriting characters, except for 12 symbols. The shapes and writing orders of the 12 symbols were defined slightly differently because some characters had a dot that cannot be expressed with eye-writing, some pairs of characters had stroke patterns too similar to discriminate, and three functional symbols needed to be defined. The predefined traces of these symbols are shown in Fig. 4. The starting point of every symbol trace was set to the center, and the participants were instructed to pause their gaze at the last point of the symbol trace before the end of the designated writing time (eight seconds per character).

C. Classification

1) *Eye-Written Character Normalization*: An eye-written trace includes the center-gazing part prior to the character writing period, and it also contains the end-point-gazing part after the character writing period. These nonmoving parts are irrelevant to the writing actions and thus must be removed from the analytical data for better classification. For eye movement detection, the gradient of the eye movement is calculated using the first-order derivative of the Gaussian function with fixed deviation (σ). Let $x_h'(t)$ be the gradient of the horizontal eye movement at a specific time t , and $x_v'(t)$ be the gradient of the vertical eye movement at a specific time t . These were defined as

$$x_h'(t) = \int_{-\infty}^{\infty} x(\tau) \cdot G'(t - \tau, \sigma) d\tau \quad (7)$$

and

$$x_v'(t) = \int_{-\infty}^{\infty} y(\tau) \cdot G'(t - \tau, \sigma) d\tau \quad (8)$$

$$\text{where } G'(t, \sigma) = -\frac{1}{\sqrt{2\pi}\sigma^3} \cdot e^{-(t^2/2\sigma^2)} \cdot t. \quad (9)$$

The nonmoving parts were detected using x_h' and x_v' . If the absolute value of the gradient for either the horizontal or the

vertical eye movement component was higher than a specific threshold (θ) at a specific time, saccadic eye movements were considered to be included in the component. In this study, we used fixed values for the slope threshold (θ) and the Gaussian function deviation (σ) over all participants, and they were empirically set to 0.05 and 8, respectively. A preliminary visual inspection of the processed signal confirmed that the selected threshold and deviation values were effective for detecting saccadic eye movements while rejecting signal fluctuations originating from noises. Since the nonmoving portions of the trace do not include any saccadic movements, the data before the first and after the last saccadic movements were truncated [Fig. 5(a) and (b)]. Then, the truncated data contained only character writing parts. The truncated time-series were then re-sampled and interpolated to have the same number of samples.

The eye-written traces of a given symbol can have variations in shapes, sizes, and positions even for a single person. The normalization of characters was conducted to overcome such variations in order to achieve better classification performance. All eye-written traces were centered at (0, 0) and resized to fit 1×1 squares while maintaining their aspect ratios [see Fig. 5(c)]. An example of reconstructed eye-written traces of all 29 symbols can be found in the Supplementary Document File.

2) *Classifiers*: To identify symbols from the normalized eye-written traces, a waveform matching technique was implemented. The input character waveform was matched against the template waveforms of every character in the symbol set, and the dissimilarity between the two waveforms was used for classification. A set of characters of a user was recorded, and his/her eye traces were preloaded as templates. By comparing the dissimilarities between the input waveform and the templates of all characters, the system determined the most similar character as the output result (see Fig. 6).

We used three different similarity (or dissimilarity) measures: Pearson's correlation, root-mean-square error (RMSE), and dynamic time warping (DTW). For the Pearson's correlation classifier, horizontal component and vertical component of the normalized eye-written traces were separated and Pearson's distances between the template and the input waveforms (1-Pearson's correlation coefficient) were calculated for both components [29]. Then, the dissimilarity (D) of Pearson's correlation classifier was defined as the sum of Pearson's distances

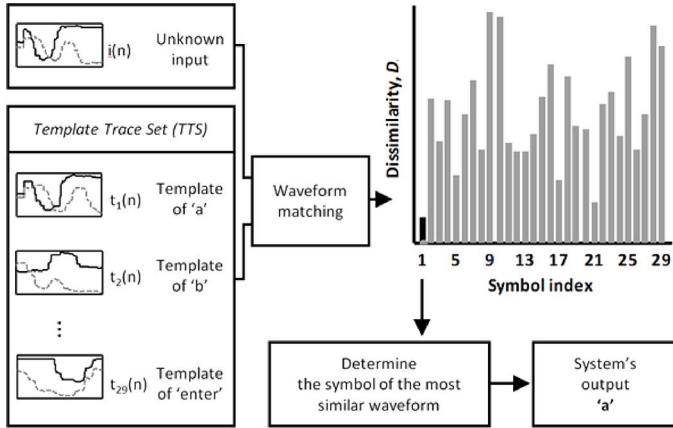


Fig. 6. Schematic of eye-written character classification. When an input gaze trace is given, it is compared to all of the templates, and the dissimilarities are calculated to determine the most probable symbol. The black bar in the graph indicates the symbol with the minimum dissimilarity.

of horizontal and vertical components. Thus, the dissimilarity (D) lies between $[0, 4]$.

The second classifier uses the RMSE as the dissimilarity measure. Horizontal component and vertical component of the normalized eye-written traces were separated and RMSE between two horizontal components (the template and the input traces) and RMSE between two vertical components (the template and the input traces) were calculated [30]. The dissimilarity (D) of RMSE classifier was defined as the sum of these horizontal and vertical RMSEs.

The third type of classifier uses DTW for two-dimensional time series to align the data points of two different time-series datasets and evaluate the dissimilarity between them [31]. The eye-written traces of the same symbol can differ in writing seed and gaze turn times. To derive a proper dissimilarity measure between two eye-written traces, DTW matches the traces point by point by warping the signals on the time axis. Then, the absolute difference between two traces that have been aligned with respect to time is calculated and used as a dissimilarity measure (D) as follows:

$$D = \sum_{n=1}^N |F(n) - G(n)| \quad (10)$$

where N indicates the number of data points in aligned waveforms, and $F(n)$ and $G(n)$ are the time-aligned waveforms of the template trace and the input trace, respectively. In this work, we used a global path constraint when calculating DTW as it limits the scope of the warping path and thus reduces the computational efforts required for path searching. The detailed explanation on the computational complexity can be found in the discussion session.

As explained earlier, an input trace is compared to the template traces of all possible symbols, and the dissimilarities are calculated using one of the three dissimilarity measures. The symbol with the minimum dissimilarity (the most similar one) is chosen to be the most probable input symbol, and it becomes the system's output for character recognition.

III. EXPERIMENT

A. Apparatus

EOG signals were acquired using a commercial multichannel bio-potential measurement system (ActiveTwo, BioSemi, Inc., Amsterdam, Netherlands). A laptop computer (4G-RAM, Intel Core i5-6300HQ 2.30 GHz CPU) was used for all experiments and computation time analyses. Real-time data recording and signal processing programs were implemented in MATLAB (Release 2013a, MathWorks, Inc., Natick, MA, USA). The MATLAB Psychophysics Toolbox [32] and its extensions were used to accurately represent controlled visual stimuli on the monitor in time, as MPC requires synchronization between stimulus timing and signal recording.

Flat active Ag/AgCl electrodes were attached to the skin surface with disposable adhesive patches. Conductive gel was also used to reduce the contact impedance between the skin surface and the electrodes. The experiments were performed 15 minutes after electrode placement in order to allow the impedance between the skin surface and the electrodes to stabilize. Two horizontal component electrodes and two vertical component electrodes were used for the EOG recordings [see Fig. 2(a)], and the left and right mastoid electrodes were used as a reference and a ground, respectively.

B. Subjects

Twenty healthy participants (14 males and six females, aged 22 ± 2.80 years) who signed consent agreements were enrolled in our study. All participants were fully informed of all experimental procedures. None of the participants had any known neurological or ophthalmic diseases such as cataracts, glaucoma, color blindness, squint, diplopia, or visual agnosia, which could affect the visual field. Eleven of them had minor refractive errors such as myopia and hyperopia. Those who had such vision problems wore glasses or contact lenses during the experiment in order to correct refractive errors.

C. Session Design

The overall experiment was composed of three sessions: a parameter calibration session, a practice session, and a data acquisition session. All parameters related to preprocessing were determined during the parameter calibration session. An EOG signal was recorded for the first 15 seconds while participants were instructed to blink their eyes naturally. The parameters for eye blink detection (i.e., blink spike threshold) were determined using the spikes evoked by the eye blinks during this time. In addition, the MPC to determine the transfer function was also performed during this session. Participants sat in front of a computer monitor at a fixed distance of 50 centimeters. The position of the monitor screen was adjusted such that its center point was at the eye level of each participant. Participants were told to focus on the white dot presented on the screen and not to turn their heads. A white dot was presented on the screen in each of nine different predefined gaze positions in a randomized order. During this, an EOG signal was recorded and used to evaluate the transfer function in (5). The inverse matrix of the transfer function was then used to reconstruct the gaze positions based on the EOG amplitudes for the subsequent sessions.

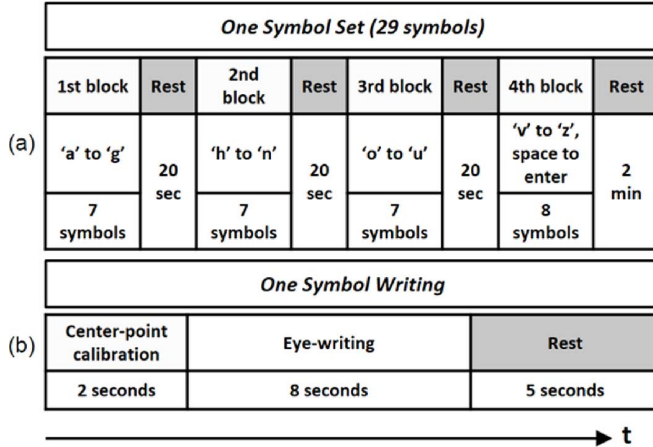


Fig. 7. Overall experimental design for data acquisition. (a) A symbol set is composed of four blocks, and 20 seconds of rest was given to participants after each block. (b) An instance of symbol writing is composed of center-point calibration, eye-writing, and rest, which is followed by the next symbol writing.

For the practice session, participants were asked to face a white empty panel for eye-writing training (see Fig. 2(b) for panel placement details). The panel had a center point indicator (a pin) for center-point calibration. Participants were instructed to eye-write symbols on the panel in such a way that the imaginary symbol trace would fill the panel. Also, auditory instructions and beeping sounds were used to cue the participants when to start eye-writing and when to finish, since there was no monitor screen visible during the eye-writing. Before the data were recorded, participants wrote a set of all of the symbols as a practice to accustom them to eye-writing.

During the data acquisition session, every participant eye-wrote five symbol sets. Each symbol set was divided into four blocks to allow sufficient resting time [Fig. 7(a)]. Each symbol writing session was composed of two seconds of center-point calibration, eight seconds of eye-writing, and five seconds of rest [Fig. 7(b)]. Twenty seconds of rest was provided between each pair of blocks in order to reduce the effects of accumulated fatigue on the eye-writing task. For the same reason, two minutes of rest were provided between the sets.

D. Classification Performance Evaluation

The eye-writing recognition system was evaluated using a leave-one-out cross validation scheme. One of five recorded eye-written symbol sets of a participant was set aside as a template set. The remaining four symbol sets were then classified using the template set and waveform matching methods described in the previous section. This process was repeated five times so that each of the datasets could be used as the template set. Thus, it generated ${}_5P_2 (= 20)$ combinations of template and test sets. The system performance was then averaged over all 20 cases for each participant and was expressed in terms of precision, recall, and F1 score. For each symbol, the precision, recall, and F1 score were calculated as

$$\text{Precision} = \frac{|TP|}{(|TP| + |FP|)} \quad (11)$$

$$\text{Recall} = \frac{|TP|}{(|TP| + |FN|)} \quad (12)$$

TABLE I
AVERAGE CLASSIFICATION PERFORMANCE OF DIFFERENT WAVEFORM MATCHING METHODS

	Waveform matching method		
	Pearson's Correlation	RMSE	DTW
Precision (%)	49.26 ± 9.61	59.65 ± 8.46	87.77 ± 7.30
Recall (%)	45.32 ± 10.30	56.03 ± 9.05	86.99 ± 7.50
F1 score (%)	47.18 ± 9.97	57.77 ± 8.75	87.38 ± 7.40

$$\text{and } F1 \text{ score} = 2 \cdot \frac{\text{Precision} \cdot \text{Recall}}{\text{Precision} + \text{Recall}} \quad (13)$$

where $|TP|$, $|FP|$, and $|FN|$ are the number of true positives, false positives, and false negatives, respectively.

Then, the precision, recall, and F1 score were averaged over all symbols to evaluate a person's average eye-writing performance. The performances of all participants were also averaged to evaluate the overall performance of the system.

IV. RESULTS

A. Average Performance

Table I shows the average classification performance of all participants using three different waveform matching methods in terms of precision, recall, and F1 score. The DTW-based classifier demonstrated the best classification performance among the three classifiers. Its averaged precision over all participants was 87.77% and the averaged recall was 86.99%. The average F1 score of the DTW-based classifier was 87.38% (see Table I). Since the DTW outperformed the other two methods, we utilized DTW for our further analyses. The performance of the DTW-based classifier for all participants is summarized in Table II. The participants with the best and worst classification results are marked in bold. The minimum accuracies (precision, recall, and F1 score) were recorded by the same participant and were much worse than those of the second worst performance (F1 score = 79.09%).

B. Summed Confusion Matrix

To identify frequently occurring errors of the recognition system, a summed confusion matrix was utilized for all participants (see Fig. 8). Each cell in the matrix represents the rate of misclassification of a given symbol (row) as another (column). The error rate of a predicted symbol x with a given true symbol y is defined as

$$\text{Error rate (symbol } x \mid \text{true symbol } y) = \frac{N(\text{predict} = x, \text{true} = y)}{N(\text{true} = y)} \quad (14)$$

where $N(\text{true} = y)$ indicates the number of eye-written traces whose true symbol is y , and $N(\text{predict} = x, \text{true} = y)$ indicates the number of eye-written traces whose true symbol is y but predicted as a symbol x . For instance, the matrix indicates that the error rate of classifying an input of “a” as “q” is between 1% and 4%. The actual value was 3.5%, and this means any input of “a” has a 3.5% possibility of being classified as “q”. Note that

TABLE II
DTW WAVEFORM MATCHING CLASSIFICATION RESULTS FOR
EACH PARTICIPANT

Participant	Precision (%)	Recall (%)	F1 score (%)
S1 (f)	79.75	78.79	79.27
S2 (m)	88.22	87.24	87.73
S3 (f)	93.63	92.59	93.10
S4 (m)	83.82	83.62	83.72
S5 (m)	93.38	92.76	93.07
S6 (m)	80.28	77.93	79.09
S7 (f)	80.61	79.83	80.22
S8 (m)	90.27	90.00	90.14
S9 (m)	91.37	90.69	91.03
S10 (m)	94.98	94.31	94.64
S11 (m)	89.46	89.14	89.30
S12 (m)	92.04	91.38	91.71
S13 (m)	88.50	87.76	88.13
S14 (f)	81.05	80.00	80.52
S15 (f)	91.01	90.00	90.50
S16 (m)	66.50	65.52	66.00
S17 (m)	86.85	86.03	86.44
S18 (f)	98.04	97.59	97.81
S19 (m)	91.93	91.55	91.74
S20 (m)	93.59	93.10	93.35
Average	87.77	86.99	87.38
Std. Dev.	7.30	7.50	7.40

* 'f' and 'm' refer to female and male participants, respectively.

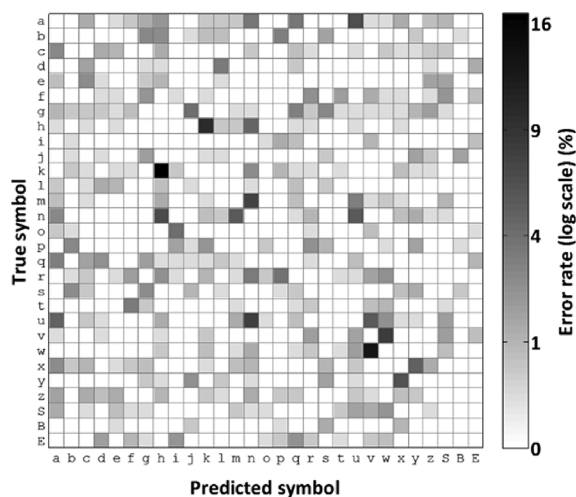


Fig. 8. Summed confusion matrix over all participants. Diagonal components were omitted. The error rate indicates the possibility of classifying an input of a given symbol (row) as another symbol (column). Upper case S, B, and E represent space, backspace, and enter, respectively. Please note that a darker color indicates a higher error rate, and the color bar is given in a log scale.

the sum of the values in one row represents the total error rate ($100 - \text{recall}$) of a given symbol (row) and that the color bar in the figure is in logarithmic scale. The most frequent error was classifying the input of “k” as “h,” with an error rate of 16.75%;

this was followed by an error of classifying “w” as “v” with an error rate of 13.25%.

1) *DTW Classification Results for Each Symbol*: The accuracies for each symbol are presented in Table III. The upper case S, B, and E represent space, backspace, and enter, respectively. The symbols showing the maximum and the minimum accuracies are marked in bold. Most of the symbols had both recall and precision in the range of 85% to 100%. The average precision over all symbols was 87.25%, and the average recall was 86.99%. A minimum precision of 68.39% was reported for the letter “h,” and a minimum recall of 73.25% was reported for the letter “u.” In contrast, a maximum precision of 97.92% was recorded for the letter “o,” and a maximum recall of 96.75% was recorded for the symbol “backspace.” A demonstration of the online eye-writing can be found on YouTube.¹

V. DISCUSSION

A. DTW Classification Results Over Different Participants

The results of eye-writing recognition using DTW indicate that the performance of the proposed system was robust across participants. Different participants demonstrated variability in writing style, eye moving speed, eye blinking frequency, stroke order for symbols, aspect ratios of characters, and EOG signal amplitudes. For instance, some participants eye-wrote symbols quickly using relatively large leaps (focus jumps) rather than gradual transitions when drawing lines. Others eye-wrote symbols slowly with smaller focus jumps (gradual transitions in focus when drawing lines). Examples of this difference in eye-writing speed among participants are illustrated in Fig. 9. Despite such large inter-individual variability, the developed eye-writing recognition system achieved a high average F1 score of 87.38% and a maximum F1 score of 97.81%. Half of the participants achieved F1 scores higher than 90%, which ranged from 90.14% to 97.81%. In addition, all participants except one achieved greater than 75% precision and recall.

One participant (subject 16 in Table II), however, exhibited poor performance with an F1 score lower than 70%. The main reason for the low accuracy was inconsistency in eye-written traces. Since our system assumes that a person has consistency in stroke orders and shapes for a given symbol when eye-writing, all participants were instructed to maintain these consistently while writing the five sets of symbols. This participant maintained such consistency for most of the symbols; however, several symbols were written in different ways (with regard to writing order and shape), which resulted in system confusion. For instance, this participant wrote the letter “p” from top to bottom three times and then wrote the same letter in the reverse order twice. This problem might be caused by lack of concentration on the task over the long experiment duration and/or the lack of sufficient practice. We expect that these types of errors would be reduced if users are given sufficient practice and rest. In this way, users would be able to become accustomed to eye-writing and adapt their eye movements to the system.

¹https://www.youtube.com/watch?v=_aKkYsvqe8k

TABLE III
DTW WAVEFORM MATCHING CLASSIFICATION RESULTS FOR EACH SYMBOL

(%)	Precision	Recall		Precision	Recall		Precision	Recall
a	77.22	76.25	l	92.65	94.50	w	81.52	80.50
b	91.88	87.75	m	89.15	84.25	x	86.96	85.00
c	88.02	90.00	n	68.66	74.50	y	87.19	88.50
d	91.15	92.75	o	97.92	94.00	z	92.25	89.25
e	93.86	91.75	p	89.31	87.75	S	89.19	90.75
f	91.45	88.25	q	85.19	87.75	B	97.48	96.75
g	84.46	81.50	r	88.62	81.75	E	94.99	90.00
h	68.39	82.75	s	90.00	90.00			
i	91.63	95.75	t	96.38	93.25			
j	91.42	93.25	u	76.30	73.25	Avg.	87.25	86.99
k	80.85	76.00	v	76.06	85.00			

* Uppercase S, B, and E represent space, backspace, and enter, respectively. The maximum and minimum values in each column are denoted by bold characters.

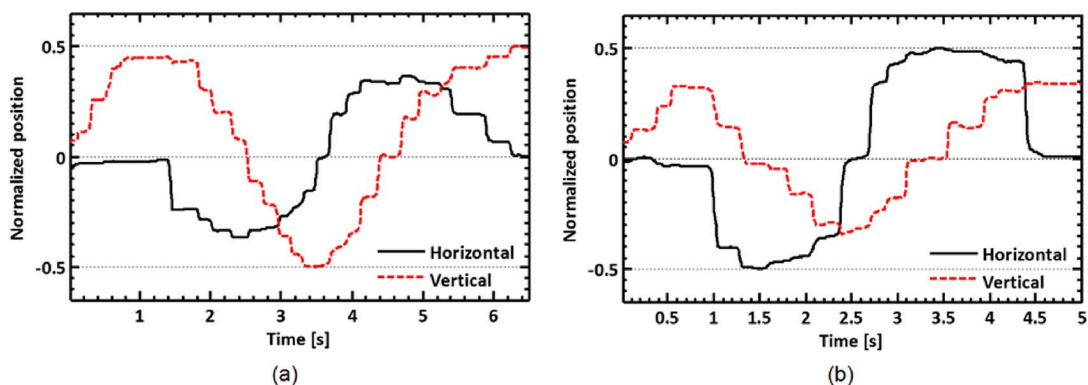


Fig. 9. Two exemplar traces from different participants, which show large inter-individual variability in eye-writing. (a) An exemplar eye-written trace of the letter “o” that was written with gradual transitions of focus. (b) An exemplar eye-written trace of the letter “o” that was written with relatively large focus jumps. Please note that these two traces have different focus jump sizes and aspect ratios (the ratio of width to height).

B. Recognition Rate of Each Symbol

The recognition rate of each symbol (Table III) was well-balanced, demonstrating the high reliability of the system. The average performance of 87.25% precision and 86.99% recall was not driven by any particular symbols with extremely high recognition rates. No single symbol had precision and recall values lower than 65%, and the recognition rates of most of the symbols ranged from 75% to 95%. This balanced distribution of recognition rates is particularly significant when evaluating multiclass classifiers.

C. Confusion Analysis

From the summed confusion matrix in Fig. 8, we identified some highly probable errors. These errors (errors with high error rates) affected the precision and recall of the error-involved symbols significantly (Table III). For instance, the most frequent error was classifying “k” as “h,” with an error rate of 16.75%. As a result, the precision of the symbol “h” was lowered, and it exhibited the minimum precision among all of the symbols. In addition, this error lowered the recall of the symbol “k” to 76%. Other examples include classifying “w” as “v,” “h” as “k,” “v” as “w,” “m” as “n,” “u” as “n,” “n” as “h,” and “a” as “u.” As one might expect, the morphological similarities between these symbol pairs are the possible cause of confusion.

Although DTW showed the best performance in classification accuracy, it could also be a source of another error. Since DTW skips several points of a waveform, some visually different character pairs such as “k” and “h,” “v” and “w,” or “m” and “n” might have high similarity. The use of additional features could be a possible solution to reduce this type of error.

Another type of error was caused by the shapes of characters. Seemingly distinguishable characters such as “u” and “n” or “a” and “u” can look similar when written in eye-writing form. For instance, the symbol “a” was most misrecognized as “u,” with an error rate of 6.5%, and “u” was misrecognized as “a” at an error rate 4.75% (see Fig. 8). The relatively high error rates in differentiating “a” and “u” come from the morphological similarity of the two eye-written traces. These symbols might not seem similar to each other in typed form or in hand-written form; however, in the eye-writing system, the user starts every eye-written trace from the center point, and eye-writing cannot represent discontinuity (pen-up and -down in handwriting) in symbol traces. These factors allow seemingly distinguishable symbols to share a significant portion of their traces in eye-written form (Fig. 10). Consequently, waveform matching might fail to clearly distinguish between the eye-written traces of such symbols. Although we expected this type of error and prepared a solution by predefining the traces of certain symbols (see Fig. 4), variability in writing order and

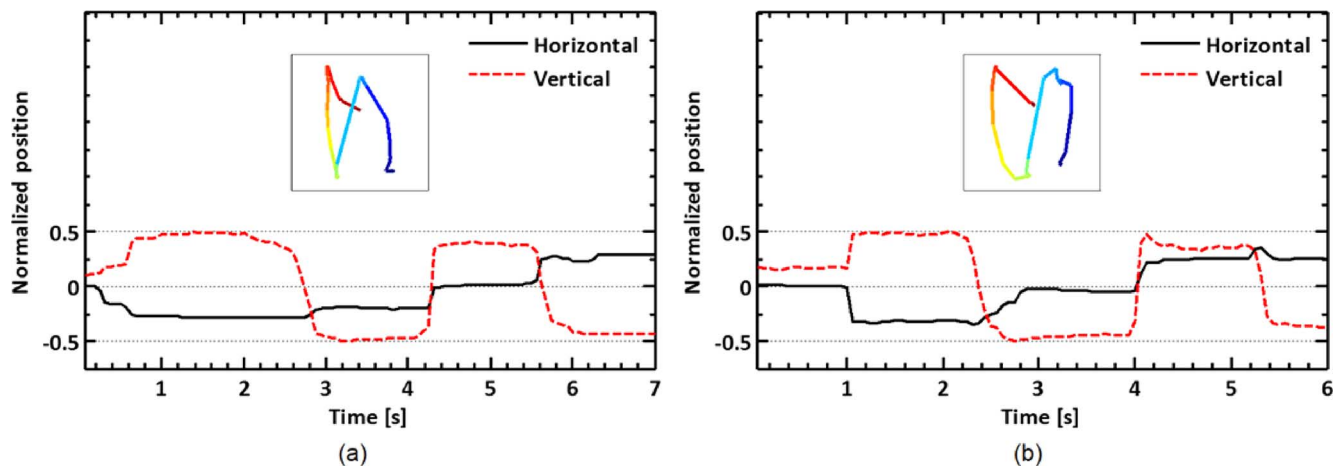


Fig. 10. Example of two letters (“n” and “u”) that have similar shapes in eye-written form. (a) An exemplar “n” character trace. (b) An exemplar “u” character trace. The center box in each figure contains the reconstructed eye-written symbol. Its colors indicate the stroke order (from red to blue).

shape among participants still generated this type of error. To avoid this error, the predefined traces would be required for more symbols.

D. Computational Cost

The proposed system incorporates a number of preprocessing procedures such as noise filtering, baseline drift removal, eye blink removal, and EMG removal. For the implementation of a real-time system, time taken for signal processing should be less than the signal sample spacing (1/128 seconds). To reduce the computational cost, we downsampled EOG signals and used an efficient artifact detection algorithm. We measured time taken for preprocessing (from data acquisition to eye-written trace reconstruction) in a laptop environment (4 GB RAM, Intel Core i5-6300HQ 2.3 GHz CPU), and the results showed that the mean preprocessing time for a data point was 0.38 ms with the standard deviation of 0.12 ms, which is about 1/20 of the signal sample spacing.

In addition, we reduced the computational cost required for DTW. The original DTW algorithm had quadratic time and space complexity [33]. To reduce this computational cost, we used a global path constraint (especially, Itakura Parallelogram [34]) when calculating a dissimilarity table. The global path constraint limits the scope of the possible warping path and thus reduces the computational efforts required for path searching. The mean classification time, which was calculated with all participants' data, was only 68.2 ms per one eye-written trace identification (max: 108.1 ms, min: 65.2 ms). Thus, the eye-writing classification results could be presented immediately to the user without any inconvenient delay.

E. Advantages

The proposed EOG-based eye-writing system has three main advantages. First, although there have been previous studies on the estimation of single, momentary movement of the eyes using EOG, methods to continuously track eye movements and estimate eye movement patterns in real time have not been reported. The suggested system offers a way to reconstruct a user's eye-written trace from an EOG signal in real time. This can be utilized to visualize the user's eye-writing input in real

time. For illustration, our current system can also be utilized without a character recognition module. In that way, users of our system can draw things freely with their eye movements and express their artistic ideas or notions without any restrictions on possible input patterns. We hope this will offer the users a creative way to express themselves. Second, the developed system requires only low computational power compared to camera-based eye trackers that require ample image processing. Consequently, the system can be implemented to develop relatively low-cost and low-power embedded systems for various purposes. For instance, the system can be applied to inexpensive communication applications for patients with ALS. Lastly, eye-writing offers a versatile and useful way to communicate with a computer. As studied earlier, the eye-writing method allows for versatile and useful eye movement-based HCI [19]. For example, the eye-writing method does not require a display on which to illustrate a virtual keyboard or command window. Thus, the system can be more easily implemented on a mobile platform. Furthermore, although each alphabet symbol trace represented an actual alphabet letter input in this work, the system can be modified so that a symbol represents any designated useful function of an HCI system. For example, when controlling an assistive robot using eye movements, the system can be designed so that an eye-writing symbol input represents any designated function of the robot. In that way, the eye-writing system will increase the speed and usability of HCI systems.

F. Limitations and Future Works

This work specifically focused on eye-writing recognition in a stationary environment. Participants sat on a chair and were instructed to stay “naturally motionless” while eye-writing. Also, users were required to face a monitor when eye-writing characters. Although the current setting is still promising for use in patients with ALS, the system needs more improvements to be applied to dynamic real-world conditions. First, the use of a monitor should be avoided to allow the system to be used in dynamic environments. In our experiment, the purpose of the monitor was to act as a “grid guide” and to assist the users in eye-writing. Without the monitor, novice users

reported trouble with knowing where to look in order to write what they intended. However, we believe that adapted users would not require the monitor to use the system. Thus, given sufficient training and adaptation time, users would be able to use the system without the guide monitor or panel. Second, any motion of a human user can generate artifacts on the EOG signal and affect eye movement detection [14]. Thus, for future applications to dynamic conditions, compensation for motion and head movements is required. Human motion detectors and motion classifiers based on accelerometers could be a possible solution to this problem [30], [31], [35]. By applying such existing systems, an EOG signal accompanied by excessive body motions could be rejected or appropriately adjusted. Lastly, in this work, all of the electrodes were connected to a commercial data acquisition platform through cables. However, the cables might cause user discomfort under dynamic real-world conditions. Headband [25] or goggle [14] type electrode embedded systems would be helpful for future applications.

In addition, experiments with patients with LIS are necessary in future studies. Although this study showed that our system works reliably for normal persons, eye-writing could be tedious and more challenging for the patient group who generally has a difficulty in moving their eyes. Thus, technical improvements would be required based on the feedback from patients.

VI. CONCLUSION

We proposed an EOG-based eye-writing recognition system for real-time environments. Participants were able to eye-write letters with volitional eye movements after a brief training period. The results of this work led us to two main conclusions. First, eye-written traces can be reconstructed from EOG signals in a real-time environment using the proposed gaze reconstruction method. Second, our experiments showed that EOG-based eye-writing has the potential to be used as an input source for HCI with diverse input patterns and reliable recognition rates. Our eye-writing recognition system is expected to be used for general HCI purposes, and it can offer a creative method of communication for patients with ALS.

REFERENCES

- [1] R. J. Krauzlis, "The control of voluntary eye movements: New perspectives," *Neuroscientist*, vol. 11, no. 2, pp. 124–137, 2005.
- [2] Q. Ding, K. Tong, and G. Li, "Development of an EOG (Electro-Oculography) based human-computer interface," *Proc. IEEE Conf. Eng. Medicine and Biology Soc.*, vol. 7, pp. 6829–6831, 2005.
- [3] R. J. K. Jacob and K. S. Karn, "Eye tracking in human-computer interaction and usability research: Ready to deliver the promises," *Mind's Eye Cogn. Appl. Asp. Eye Mov. Res.*, pp. 573–605, 2003.
- [4] A. E. Kaufman, A. Bandopadhyay, and B. D. Shaviv, "An eye tracking computer user interface," in *Proc. IEEE Res. Properties in Virtual Reality Symp.*, 1993, pp. 120–121.
- [5] Y. Tomita, Y. Igarashi, S. Honda, and N. Matsuo, "Electro-oculography mouse for amyotrophic lateral sclerosis patients," in *Proc. 18th Annu. Int. Conf. IEEE Eng. Medicine and Biology Soc.*, 1996, pp. 1780–1781.
- [6] W. S. Wijesoma, K. S. Wee, O. C. Wee, A. P. Balasuriya, K. T. San, and L. K. Soon, "EOG based control of mobile assistive platforms for the severely disabled," in *Proc. IEEE Int. Conf. Robotics and Biomimetics*, 2005, pp. 490–494.
- [7] L. Y. Deng, C.-L. Hsu, T.-C. Lin, J.-S. Tuan, and S.-M. Chang, "EOG-based Human-Computer Interface system development," *Expert Syst. Appl.*, vol. 37, no. 4, pp. 3337–3343, 2010.
- [8] D. Hirtz, D. J. Thurman, K. Gwinn-Hardy, M. Mohamed, a. R. Chaudhuri, and R. Zalutsky, "How common are the 'common' neurologic disorders?," *Neurology*, vol. 68, no. 5, pp. 326–337, 2007.
- [9] A. Brockington, K. Ning, P. R. Heath, E. Wood, J. Kirby, N. Fusi, N. Lawrence, S. B. Wharton, P. G. Ince, and P. J. Shaw, "Unravelling the enigma of selective vulnerability in neurodegeneration: Motor neurons resistant to degeneration in ALS show distinct gene expression characteristics and decreased susceptibility to excitotoxicity," *Acta Neuropathol.*, vol. 125, no. 1, pp. 95–109, 2013.
- [10] H. D. Crane and C. M. Steele, "Generation-V dual-Purkinje-image eye-tracker," *Appl. Opt.*, vol. 24, no. 4, pp. 527–537, 1985.
- [11] H. Hua, P. Krishnaswamy, and J. P. Rolland, "Video-based eyetracking methods and algorithms in head-mounted displays," *Opt. Express*, vol. 14, no. 10, pp. 4328–4350, 2006.
- [12] W. Heide, E. Koenig, P. Trillenber, D. Kömpf, and D. S. Zee, *Electrooculography: Technical Standards and Applications. Int. Federation of Clinical Neurophysiology*, vol. 52, 1999.
- [13] C. H. Morimoto and M. R. M. Mimica, "Eye gaze tracking techniques for interactive applications," *Comput. Vis. Image Underst.*, vol. 98, pp. 4–24, 2005.
- [14] A. Bulling, D. Roggen, and G. Tröster, "Wearable EOG goggles: Seamless sensing and context-awareness in everyday environments," *J. Ambient Intell. Smart Environ.*, vol. 1, no. 2, pp. 157–171, 2009.
- [15] R. Barea, L. Boquete, M. Mazo, and E. López, "Wheelchair guidance strategies using EOG," *J. Intell. Robot. Syst. Theory Appl.*, vol. 34, pp. 279–299, 2002.
- [16] C. H. Kuo, Y. C. Chan, H. C. Chou, and J. W. Siao, "Eyeglasses based electrooculography human-wheelchair interface," in *Proc. IEEE Int. Conf. Syst. Man Cybern.*, Oct. 2009, pp. 4746–4751.
- [17] K. Yamagishi, J. Hori, and M. Miyakawa, "Development of EOG-based communication system controlled by eight-directional eye movements," in *Proc. Annu. Int. Conf. IEEE Engineering in Medicine and Biology*, 2006, pp. 2574–2577.
- [18] A. Bulling, J. A. Ward, H. Gellersen, and G. Tröster, "Eye movement analysis for activity recognition using electrooculography," *IEEE Trans. Pattern Anal. Mach. Intell.*, vol. 33, no. 1, pp. 741–753, 2011.
- [19] J.-Z. Tsai, C.-K. Lee, C.-M. Wu, J.-J. Wu, and K.-P. Kao, "A feasibility study of an eye-writing system based on electro-oculography," *J. Med. Biol. Eng.*, vol. 28, no. 1, pp. 39–46, 2008.
- [20] K. Pettersson, S. Jagadeesan, K. Lukander, A. Henelius, E. Haegström, and K. Müller, "Algorithm for automatic analysis of electro-oculographic data," *Biomed. Eng. Online*, vol. 12, no. 110, pp. 1–17, 2013.
- [21] S. Ge, M. Han, and X. Hong, "A fully automatic ocular artifact removal from EEG based on fourth-order tensor method," *Biomed. Eng. Lett.*, vol. 4, pp. 68–76, 2014.
- [22] W.-D. Chang, H.-S. Cha, K. Kim, and C.-H. Im, "Detection of eye blink artifacts from single prefrontal channel electroencephalogram," *Comput. Methods Programs Biomed.*, 2015.
- [23] W.-D. Chang, J.-H. Lim, and C.-H. Im, "An unsupervised eye blink detection method for real-time electroencephalogram processing," *Physiol. Meas.*, 2016, to be published.
- [24] L. Lindström, R. Magnussen, and I. Petersen, "Muscular fatigue and action potential conduction velocity changes studied with frequency analysis of EMG signals," *Electromyography*, vol. 10, no. 4, pp. 341–356, 1970.
- [25] F. Simini, A. Touya, A. Senatore, and J. Pereira, "Gaze tracker by electrooculography (EOG) on a head-band," in *Proc. 10th Int. Workshop Biomedical Eng.*, 2011, pp. 1–4.
- [26] D. Kumar and E. Poole, "Classification of EOG for human computer interface," in *Proc. 24th Annu. Conf. Fall Meeting Biomedical Eng. Soc. EMBS/BMES*, 2002, vol. 1, pp. 64–67.
- [27] T. Yagi, Y. Kuno, K. Koga, and T. Mukai, "Drifting and blinking compensation in electro-oculography (EOG) eye-gaze interface," in *Proc. IEEE Int. Conf. Systems, Man and Cybernetics*, 2007, vol. 4, pp. 3222–3226.
- [28] D. H. Lee, J. H. Yu, and D. H. Kim, "Extraction of gaze point on display based on EOG for general paralysis patient," *Rehabil. Eng. Assist. Technol. Soc. Korea*, vol. 5, no. 1, pp. 88–93, 2011.
- [29] J. Benesty, J. Chen, Y. Huang, and I. Cohen, *Pearson Correlation Coefficient*, vol. 2, 2009.
- [30] Z. Wang and A. C. Bovik, "Mean squared error: Lot it or leave it? A new look at signal fidelity measures," *IEEE Signal Process. Mag.*, vol. 26, no. 1, pp. 98–117, 2009.
- [31] K. R. Anderson and J. E. Gaby, "Dynamic waveform matching," *Inf. Sci. (Nj.)*, vol. 31, pp. 221–242, 1983.

- [32] D. G. Pelli, "The VideoToolbox software for visual psychophysics: Transforming numbers into movies," *Spat. Vis.*, vol. 10, no. 4, pp. 437–442, 1997.
- [33] C. Ratanamahatana and E. Keogh, "Making time-series classification more accurate using learned constraints," in *Proc. Sdm Int. Conf.*, 2004, pp. 11–22.
- [34] L. Rabiner and B.-H. Juang, *Fundamentals of Speech Recognition*, vol. 103, 1993.
- [35] U. Jensen, H. Leutheuser, S. Hofmann, B. Schuepferling, G. Suttner, K. Seiler, J. Kornhuber, and B. M. Eskofier, "A wearable real-time activity tracker," *Biomed. Eng. Lett.*, vol. 5, no. 4, pp. 147–157, Apr. 2015.

Kwang-Ryeol Lee received the B.Eng. degree in bio and brain engineering from Korea Advanced Institute of Science and Technology, Korea, in 2015.

He spent six months working as a Visiting Researcher at Brown University, Providence, RI, USA. He collaborated with the Computational Neuroengineering Lab, Hanyang University, Korea for this research. His research interests include human-computer interaction and its application in the biomedical field.

Won-Du Chang received the M.Sc. degree in computer science and engineering from Pusan National University, Korea, in 2005, and the Ph.D. degree from the Department of Computer Science and Engineering, University of Aizu, Japan, in 2011.

Until 2013, he worked as an Assistant Professor at Mongolia International University, Mongolia. Currently, he is a Research Assistant Professor in the Department of Biomedical Engineering, Hanyang University, Korea. His research interests include biomedical signal analysis and pattern detection/recognition in time-series signals.

Sungkean Kim received the B.S. and M.S. degrees in biomedical engineering from Yonsei University, Korea. He is working toward the Ph.D. degree in the Department of Biomedical Engineering, Hanyang University, Korea.

His research interests include the diagnosis of psychiatric diseases using brain signals and brain signal analysis.

Chang-Hwan Im (M'09) graduated from the School of Electrical Engineering, Seoul National University, Korea, in 1999, and received the M.S. and Ph.D. degrees from the same university in 2001 and 2005, respectively.

He worked as a Postdoctoral Associate in the Department of Biomedical Engineering, University of Minnesota, Minneapolis, MN, USA, from 2005 to 2006. From 2006 to 2011, he worked for the Department of Biomedical Engineering, Yonsei University, Korea, as an Assistant/Associate Professor. Since 2011, he has been working for the Department of Biomedical Engineering, Hanyang University, Korea, as an Associate Professor. His research interests cover various fields of neuroelectromagnetics and computational neuroengineering, especially brain-computer interfaces, the diagnosis of neuropsychiatric diseases, noninvasive brain stimulation, bioelectromagnetic source imaging, and dynamic neuroimaging. He has authored more than 120 articles in peer-reviewed international journals. He is currently a Director of the Computational Neuroengineering Laboratory of Hanyang University.